Proceedings of the
47th IEEE Conference on Decision and Control
Cancun, Mexico, Dec. 9-11, 2008

Optimising the braking performance via nonlinear analysis and bifurcation theory

Mara Tanelli, Alessandra Gragnani, Alessandro Astolfi and Sergio M. Savaresi

Abstract— **This paper shows how the properties of a recently proposed nonlinear output feedback controller for active braking control systems can be exploited to optimise the braking performance. The control algorithm, in fact, allows to detect in which region of the friction curve the system is operating. Thus, via nonlinear analysis and bifurcation theory, we show that the closed-loop system exhibits a supercritical Hopf bifurcation. Based on this, we propose a way to estimate the current road conditions and to adapt the set-point in order to optimise the braking performance. A bifurcation diagram is also worked out to study the closed-loop dynamics modifications due to possible actuator faults or degradations.**

I. Introduction

Electronic Anti-lock Braking Systems (ABS) have recently become a standard for all modern cars. ABS can greatly improve the safety of a vehicle, as it maximises the longitudinal tire-road friction while keeping large lateral forces which guarantee vehicle steerability. The current trend in braking control systems design is to move from threshold-based control logics, mainly based on wheel deceleration measurements, to genuine slip-control (see *e.g.*, [6], [3], [11]). The main motivation behind this major change in ABS design is due to the recent technological advances in actuators, both electro-hydraulic and electro-mechanical, which are replacing hydraulic brakes with discrete dynamics and enable a continuous modulation of the braking torque. In the field of automatic braking control many approaches have been proposed, ranging from classical regulation loops based on linearised models, to genuinely nonlinear control strategies, see *e.g.,* [3], [11], [10]. One of the main challenges in designing ABS systems is to devise control logics which are robust with respect to two significant sources of uncertainty affecting the braking dynamics: the highly nonlinear tire-road friction forces and the dynamic load transfer between front and rear axle. Many research efforts have been devoted to estimate the road characteristics on-line (see *e.g.*, [5], [2], [9]) as the knowledge of the current road conditions allows to optimise both braking performance and passengers' safety.

In this work, starting from the nonlinear output feedback controller proposed in [11], the closed-loop properties are exploited to adapt the set-point online in order to operate the system always on the peak of the tire-road friction curve, thereby optimising the braking performance. Specifically, the control algorithm in [11] is such that the closed-loop trajectories either tend to an asymptotically stable equilibrium or to an attractive limit cycle, according to the position of the set-point with respect to the friction curve peak in the current and unknown road conditions. We start by showing that the closed-loop system exhibits a supercritical Hopf bifurcation. Taking advantage of the system dynamics at the bifurcation point, we show how to adapt the set-point online and optimise the braking performance. Finally, a bifurcation diagram is worked out to consider the case in which the braking system performance degradates due to usage or faults and we analytically study the resulting closed-loop dynamics.

The work of M. Tanelli and S.M. Savaresi is partially supported by MIUR project "New methods for Identification and Adaptive Control for Industrial Systems". M. Tanelli, A. Gragnani and S.M. Savaresi are with the Dipartimento di Elettronica e Informazione, Politecnico di Milano, Piazza L. da Vinci 32, 20133 Milano, Italy. e-mail: {tanelli,gragnani,savaresi}@elet.polimi.it. M. Tanelli is also with the Dipartimento di Ingegneria dell'Informazione e Metodi Matematici, Università degli studi di Bergamo, Via Marconi 5, 24044, Dalmine (BG), Italy. Alessandro Astolfi is with the Department of Electrical and Electronic Engineering, Imperial College London, London, SW7 2AZ, UK. e-mail:a.astolfi@ic.ac.uk and with Dipartimento di Informatica, Sistemi e Produzione, Università di Roma Tor Vergata, Via del Politecnico 1, 00133 Roma, Italy.

II. System Description

For the preliminary design of braking control algorithms a simple but effective single corner model is typically used. The model is given by the following equations [6]

$$J\dot{\omega} = rF_x - T_b, \quad m\dot{v} = -F_x, \tag{1}$$

where $\omega\,[rad/s]$ is the angular speed of the wheel, $v\,[m/s]$ is the longitudinal speed of the vehicle body, $T_b\,[Nm]$ is the braking torque, $F_x\,[N]$ is the longitudinal tire-road contact force, $J\,[kg\,m^2]$, $m\,[kg]$ and $r\,[m]$ are the rotational inertia of the wheel, the quarter-car mass and the wheel radius, respectively. In the rest of the paper the following values will be employed: $J = 1\,kg\,m^2$, $r = 0.3\,m$, $m = 225\,kg$. The dynamic behavior of the system is hidden in the expression of F_x, which depends on the state variables v and ω. The most general expression of F_x is involved, since it depends on a large number of features of the road, tire, and suspension. However, it can be well-approximated as $F_x = F_z\mu(\lambda;\vartheta)$, where F_z is the vertical force at the tire-road contact point; $\lambda = (v - \omega r)/v$ is the longitudinal slip, and ϑ is a set of parameters which characterise the shape of the static function $\mu(\lambda;\vartheta)$. Many empirical analytical expressions for the function $\mu(\lambda;\vartheta)$ have been proposed; a simple and widely-used model is [7]

$$\mu(\lambda;\vartheta) = \vartheta_1(1 - e^{-\lambda\vartheta_2}) - \lambda\vartheta_3. \tag{2}$$

Note that the vector ϑ has three elements only: by changing their values many different tire-road friction conditions can be modeled. In Figure 1 the shapes of $\mu(\lambda;\vartheta)$ in four different road conditions are displayed. The parameter values for the given curves are from [7]. From now on, for simplicity, also the dependency of $\mu(\lambda;\vartheta)$ on ϑ is omitted, and the function in Equation (2) is referred to as $\mu(\lambda)$.

978-1-4244-3124-3/08/$25.00 ©2008 IEEE

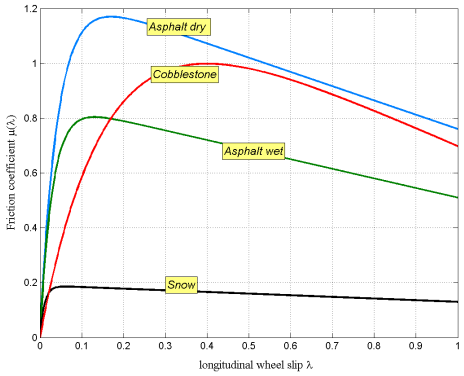

Fig. 1. Shapes of the function $\mu(\lambda;\vartheta)$ in different road conditions.

Employing the expression of F_x introduced above and substituting $\dot{\lambda} = -\frac{r}{v}\dot{\omega} + \frac{r\omega}{v^2}\dot{v}, \omega = \frac{v}{r}(1-\lambda)$ into (1) yields

$$\dot{\lambda} = -\frac{1}{v}[\frac{(1-\lambda)}{m} + \frac{r^2}{J}]F_z\mu(\lambda) + \frac{r}{vJ}T_b,\ m\dot{v} = -F_z\mu(\lambda). \quad (3)$$

In the following it is assumed (see *e.g.*, [10]) that the longitudinal dynamics of the vehicle are much slower than the rotational dynamics of the wheel due to the large difference in inertia. Hence, v is considered as a slowly-varying parameter and the second equation (describing the vehicle dynamics) of system (1) is neglected.

III. Problem Formulation and Main Assumptions

According to the assumption on the vehicle speed and expressing v as $v = \frac{\omega r}{1-\lambda}$, the system dynamics are given by

$$\dot{\lambda} = -\frac{1-\lambda}{J\omega}(\Psi(\lambda) - T_b), \quad (4)$$

with $\omega \geq 0$ and

$$\Psi(\lambda) = \left(r + \frac{J}{rm}(1-\lambda)\right)F_z\mu(\lambda). \quad (5)$$

When $\mu(\lambda)$ is as in (2) and the control input is constant *i.e.*, $T_b = T_b^{ss} \geq 0$, the system exhibits the following equilibria (see Figure 2): 1) if $T_b^{ss} > \max_\lambda \Psi(\lambda)$, the unique equilibrium

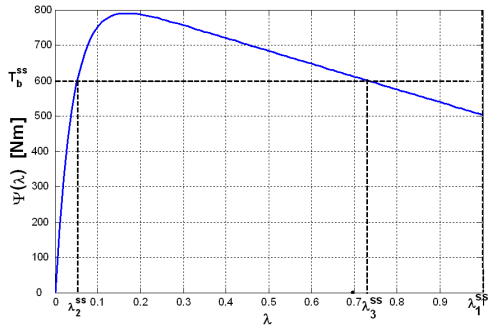

Fig. 2. Equilibrium points for the quarter-car system (4).

point is $\lambda_1^{ss} = 1$; 2) if $T_b^{ss} \leq \max_\lambda \Psi(\lambda)$, the system has at most three equilibria, namely $\lambda_1^{ss} = 1$, $\lambda_2^{ss} = \bar{\lambda}_2$ and $\lambda_3^{ss} = \bar{\lambda}_3$, where $\bar{\lambda}_2 \leq \bar{\lambda}_3$ are the two possibly coincident solutions of $T_b^{ss} = \Psi(\lambda)$, as shown in Figure 2. Note that, for any control input $T_b \geq 0$, the state variable is non-negative, *i.e.*, $\lambda \geq 0$. In fact, for non-negative braking torques, the vehicle is either at constant speed or it is braking, and $\lambda \in [0,1]$ during braking. In the following, we work under the following assumptions. **A1)** The control input T_b takes values in a non-empty subset of the non-negative real axis, *i.e.*, $T_b \in [\underline{T}_b, \overline{T}_b]$, for some known values $\underline{T}_b$ and $\overline{T}_b$ such that $0 \leq \underline{T}_b < \overline{T}_b$. Note that this hypothesis is always verified in practice, as the values $\underline{T}_b$ and $\overline{T}_b$ are imposed by the actuator characteristics. We consider that the actuator limits $\underline{T}_b$ and $\overline{T}_b$ are such that $\underline{T}_b = 0$ and $\overline{T}_b > \max_\lambda \Psi(\lambda)$. **A2)** The longitudinal slip set-point λ^* is selected such that $T_b^* < \max_\lambda \Psi(\lambda)$. This inequality (see Figure 2) is verified for all choices of λ^*, but for the exact peak point of the $\Psi(\lambda)$ curve.

IV. Output Feedback Controller

We now briefly describe the output feedback control law presented in [11], which is a dynamic update law such that a desired equilibrium point of system (4) is robustly stabilised in the sense of Lyapunov.

Proposition 4.1: [11] Consider the quarter-car model described by Equation (4). Assume **A1)** and **A2)** hold. Let $\lambda^* \in (0,1)$ be the smallest solution of $T_b^{ss} = \Psi(\lambda)$. Suppose that either

$$\lambda_3^{ss}\left(1 + \frac{1}{\ln(1-\lambda_3^{ss})}\right) \leq \lambda^* < \lambda_3^{ss} \quad \text{or} \quad \lambda_3^{ss} \geq 1. \quad (6)$$

Then, for any $\theta(0) \in (0, \overline{T}_b)$, the dynamic output feedback control law

$$T_b = \theta, \quad \dot{\theta} = k_\lambda \frac{1}{J\omega}(\lambda - \lambda^*)(\theta - \overline{T}_b)(\theta - \underline{T}_b) \quad (7)$$

with $k_\lambda > 0$ and $\omega > 0$ is such that the equilibrium point (λ^*, θ^*) of the closed-loop system (4),(7) is *locally stable* and for any initial condition $\lambda(0)$ in the region

$$\Lambda = \{\lambda \in \mathbb{R} \mid 0 \leq \lambda \leq 1\} \quad (8)$$

$\lambda(t)$ remains in this region. Moreover, if $\lambda(0) \neq 1$, $\lambda(t)$ converges asymptotically to λ^*. Let now $\lambda^* \in (0,1)$ be the largest solution of $T_b^{ss} = \Psi(\lambda)$. Then the control law (7) is such that, for any initial condition $\lambda(0) \in \Lambda$, $\lambda(t)$ remains in this region. Moreover, if $\lambda(0) \neq 1$, the closed-loop system trajectory $(\lambda(t), \theta(t))$ converges to an attractive periodic orbit encircling the equilibrium (λ^*, θ^*).
Finally, in both cases, the control variable T_b remains in the set $[\underline{T}_b, \overline{T}_b]$ for all $t \geq 0$.

Proposition 4.1 proves that if the selected set-point λ^* is the smallest solution of $T_b^{ss} = \Psi(\lambda)$, then (λ^*, θ^*) is locally asymptotically stable. On the other hand, if λ^* is the largest solution of $T_b^{ss} = \Psi(\lambda)$, then the control law makes the closed-loop trajectory converge to an attractive periodic orbit. From (5), as $rm >> J$, we see that $\Psi(\lambda) \simeq rF_z\mu(\lambda)$. As such, the abscissa of the maximum of $\Psi(\lambda)$ is – for all practical purposes – that of the peak of the friction curve. For what follows we only need to remark that the region Λ in (8) is invariant. Furthermore, the linearisation of system (4),(7) (see [11] for details) allows to show that the boundary equilibria $(\lambda = 1, \theta = \overline{T}_b)$, $(\lambda = 1, \theta = \underline{T}_b = 0)$ are saddles,

whereas $(\lambda = 0, \theta = \underline{T}_b = 0)$ is an unstable node. Moreover, the only initial conditions yielding trajectories that converge to $(1, \overline{T}_b)$ are such that $\theta(0) = \overline{T}_b$, whereas the only initial conditions yielding trajectories that converge to $(1, \underline{T}_b)$ are such that $\lambda(0) = 1$. Accordingly, the closed-loop trajectories are such that the region

$$\mathscr{D} = \left\{(\lambda, \theta) \in \mathbb{R}^2 \mid 0 \leq \lambda < 1, \theta \in (\underline{T}_b, \overline{T}_b)\right\} \qquad (9)$$

is a *trapping* region for the closed-loop system (4),(7).

Based on these properties it is worth noting that, on one hand, the system stability and the related safety of the braking maneuver are always guaranteed while, on the other, the periodic behavior of the closed-loop trajectory can be monitored to detect if the closed-loop working condition lies in the unstable region of the friction curve. This very peculiar feature of the proposed control law can be profitably employed to adjust on-line the wheel slip set-point, once the periodic behavior is detected.

V. Computation and analysis of the Hopf bifurcation

We now exploit the closed-loop system properties to search in real-time for the wheel slip value which maximises the friction force so to always operate with the best possible braking performance. The closed-loop behavior suggests that, considering the set-point value λ^* as a bifurcation parameter, a Hopf bifurcation occurs. As such, one can exploit the properties of this bifurcation together with the amplitude and period of the limit cycle – which are in fact functions of λ^* and of the road parameters – to estimate the road conditions and adjust the set-point value accordingly. First, we show that the closed-loop system (4),(7) exhibits a supercritical Hopf bifurcation. To this end, consider the Jacobian of the closed-loop system (4),(7) evaluated at the equilibrium $\lambda = \lambda^*$ and $\theta^* = \psi(\lambda^*)$, which has the form

$$J = \begin{bmatrix} -\frac{1-\lambda^*}{J\omega} \left.\frac{d\psi}{d\lambda}\right|_{\lambda^*} & \frac{1-\lambda^*}{J\omega} \\ k_\lambda \frac{1}{J\omega}(\theta^* - \overline{T}_b)\theta^* & 0 \end{bmatrix}. \qquad (10)$$

From (10), we obtain that $\mathrm{tr}(J) = -\frac{1-\lambda^*}{J\omega} \left.\frac{d\psi(\lambda)}{d\lambda}\right|_{\lambda^*}$ and $\det(J) = -\frac{1-\lambda^*}{J\omega} k_\lambda \frac{1}{J\omega}(\theta^* - \overline{T}_b)\theta^*$. Thus, as $(1-\lambda^*) > 0$ and $(\theta^* - \overline{T}_b) < 0$ due to **A2)**, $\det(J) > 0$. As such, to have a Hopf bifurcation, we need $\mathrm{tr}(J) = 0$ [12]. This is true if $\left.\frac{d\psi}{d\lambda}\right|_{\lambda^*} = 0$, which translates into

$$-\frac{J}{rm}\mu(\lambda^*) + \left[r + \frac{J}{rm}(1-\lambda^*)\right] \left.\frac{d\mu(\lambda)}{d\lambda}\right|_{\lambda^*} = 0 \qquad (11)$$

where $\mu(\lambda)$ is as in (2). Note that, as $rm >> J$, condition (11) shows that $\lambda^*_{Hopf} \simeq \lambda_{peak}$, where λ^*_{peak} indicates the abscissa of the peak of the friction curve. In fact, λ^*_{Hopf} is slightly to the left of λ_{peak}. Thus, if we take the system to operate at λ^*_{Hopf}, we are in fact maximising the braking torque. Now that the existence of the Hopf bifurcation has been verified, it is interesting to investigate whether it is *super-* or *sub*-critical, [12], [4], [1]. A supercritical Hopf bifurcation is non-catastrophic, in the sense that, for small perturbations of the parameter values around the bifurcation condition, the system trajectories move from an attractor to a nearby other. On the contrary, a subcritical Hopf bifurcation is catastrophic, in the sense that, for small perturbations of the parameter values around the bifurcation condition, the system state suddenly jumps from an attractor to some distant one. To establish the type of the Hopf bifurcation, one needs to compute the so-called first Lyapunov coefficient [4], [1]: if it is positive, then the bifurcation is subcritical, if it is negative, then it is supercritical. If the coefficient happens to be equal to zero, then the bifurcation is said to be degenerate. To study the Hopf bifurcation, we consider the closed-loop system in the form

$$\dot{\lambda} = f_1(\lambda, \theta), \quad \dot{\theta} = f_2(\lambda, \theta). \qquad (12)$$

Then, we use the change of coordinates $\delta\lambda = \lambda - \lambda^*$ and $\delta\theta = \theta - \theta^*$ to shift the equilibrium (λ^*, θ^*) to the origin. Evaluating the Jacobian of system (12) in the new coordinate system for the value of λ^* which satisfies (11), we find that it has a simple pair of purely imaginary eigenvalues. The system dynamics can thus be written in the form

$$\begin{pmatrix} \dot{\delta\lambda} \\ \dot{\delta\theta} \end{pmatrix} = F \begin{pmatrix} \delta\lambda \\ \delta\theta \end{pmatrix} + \begin{pmatrix} g^1(\delta\lambda, \delta\theta) \\ g^2(\delta\lambda, \delta\theta) \end{pmatrix}, \qquad (13)$$

where $g^i(\delta\lambda, \delta\theta), i = 1,2$ are nonlinear in $\delta\lambda$ and $\delta\theta$. It can be shown, [12], that the functions $g^i(\delta\lambda, \delta\theta)$, $i = 1,2$ contain no even terms and that, if we consider small perturbations about the Hopf bifurcation, only the cubic terms need to be considered. The stability of the periodic orbit is then determined, [8], [12], by the sign of the first Lyapunov coefficient ℓ_1 - which represents the coefficient of the cubic terms of $g^1(\delta\lambda, \delta\theta)$ for the parameter value corresponding to the Hopf bifurcation. Namely, its expression is [4]

$$\ell_1 = \tfrac{1}{16}\left\{\left[g^1_{\delta\lambda_3} g^1_{\delta\lambda_1\delta\theta_2} + g^2_{\delta\lambda_2\delta\theta_1} + g^2_{\delta\theta_3}\right] + \tfrac{1}{\beta}\left[g^1_{\delta\lambda_1\delta\theta_2} \times \right.\right.$$
$$\left.\left. \times (g^1_{\delta\lambda_2} + g^1_{\delta\theta_2}) - g^2_{\delta\lambda_1\delta\theta_1}(g^2_{\delta\lambda_1} + g^2_{\delta\theta_2}) - g^1_{\delta\lambda_2} g^2_{\delta\lambda_2} + g^1_{\delta\theta_2} g^2_{\delta\theta_2}\right]\right\},$$

where $g^i_{x_j y_k} = \frac{\partial^{j+k} g^i(x,y)}{\partial x^j \partial y^k}$ and all partial derivatives are evaluated at the bifurcation point. For our system, the (long and tedious) calculations needed to compute ℓ_1 have been carried out with the help of a symbolic mathematical toolbox. After further re-elaboration of the results, the final expression of the first Lyapunov coefficient is

$$\ell_1 = -\frac{F_z}{16 J\omega rm}\left[4J \left.\frac{d\mu(\lambda)}{d\lambda}\right|_{\lambda^*} + J\vartheta_1\vartheta_3 e^{-\lambda^*\vartheta_2}(\lambda^* - 1)^2 + \right.$$
$$+ 5J\vartheta_1\vartheta_2^2 e^{-\lambda^*\vartheta_2}(1-\lambda^*) + \qquad (14)$$
$$\left. + r^2 m\vartheta_1\vartheta_3^2 e^{-\lambda^*\vartheta_2}(1-\lambda^*) + 2r^2 m\vartheta_1\vartheta_2^2 e^{-\lambda^*\vartheta_2}(1-\lambda^*)\right].$$

Thus, as $\lambda^* < 1$, $\left.\frac{d\mu(\lambda)}{d\lambda}\right|_{\lambda^*} > 0$ at the bifurcation point and all other parameters are positive, $\ell_1 < 0$ and the Hopf bifurcation is supercritical. Notably, this condition holds for all road conditions.

VI. Online friction estimation and braking performance optimization

We now illustrate a strategy based on the Hopf bifurcation by means of which the braking performance can be optimised by first estimating the current (unknown) road conditions and then adapting the set-point value to take the system to operate on the peak of the tire-road friction curve. Exploiting the relationships between the three parameters ϑ characterising (2), one may notice that $\vartheta_3 = \alpha\vartheta_1$, with $\alpha = 0.4065$ if dry and wet asphalt are considered. Thus, in what follows we restrict the parameter space to $(\vartheta_1, \vartheta_2)$. To estimate the road conditions we first let the braking maneuver start with a choice of the set-point λ^* such that a limit cycle exists for all road conditions. For illustration purposes, in the following we work considering the dry and wet asphalt cases and set $\lambda^* = 0.3$. Then, upon braking, we measure the amplitude[1] $\overline{A}$, the period $\overline{T}$ and the maximum value of the braking torque $\overline{\theta}_{Max}$. Then, we employ pre-computed look-up tables in which the values of the amplitude $A(\vartheta_1, \vartheta_2)$ and the period $T(\vartheta_1, \vartheta_2)$ of the limit cycle and the maximum value of the braking torque $\theta_{Max}(\vartheta_1, \vartheta_2)$ for $\lambda^* = 0.3$ in the parameter space $(\vartheta_1, \vartheta_2)$ – recall that $\vartheta_3 = \alpha\vartheta_1$ – are stored to estimate the current road conditions. Namely, we look for

$$(\vartheta_1^*, \vartheta_2^*) = \text{argmin}_{(\vartheta_1,\vartheta_2)}[(\overline{\text{A}} - \text{A}(\vartheta_1, \vartheta_2))^2 + (\overline{\text{T}} - \text{T}(\vartheta_1, \vartheta_2))^2 + (\overline{\theta}_{Max} - \theta_{Max}(\vartheta_1, \vartheta_2))^2]. \quad (15)$$

Specifically, the iso-amplitude $A(\vartheta_1, \vartheta_2) = \overline{A}$, iso-period $T(\vartheta_1, \vartheta_2) = \overline{T}$ and iso-θ_{Max} curves for dry asphalt in the parameter space $(\vartheta_1, \vartheta_2)$ for $\lambda^* = 0.3$, with a 70×70 grid have been computed. Figure 3 shows the intersections which exist for dry and wet asphalt, respectively, and the estimated $(\vartheta_1^*, \vartheta_2^*)$ pair. For readability, only the iso-amplitude and iso-period curves are shown. Note, however, that the third error component of (16), which accounts for the maximum value of the braking torque θ_{Max} on the limit cycle, is crucial to find the estimate of the correct point. Once the road

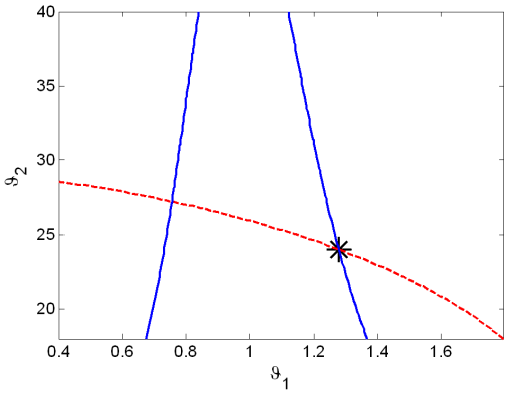

Fig. 3. Intersections between iso-amplitude (dashed line) and iso-period (solid line) curves for dry asphalt in the parameter space and estimated pair $(\vartheta_1^*, \vartheta_2^*)$ (asterisk).

conditions have been estimated, one can find the new value to assign to the set-point λ^* so that it corresponds to the bifurcation point. This is done by looking for the value of λ which maximises the function $\Psi(\lambda)$, see (11). Practically, by means of a stored matrix which contains the λ^*_{Hopf} for all $(\vartheta_1, \vartheta_2)$, we need only to query the corresponding look-up table. As an indication, with a 70×70 matrix, we have a relative percentage estimation error in the λ^*_{Hopf} value of 0.1%. In braking control applications, it is crucial that the control algorithm can correctly manage sudden changes in the road conditions (called μ-jumps), which possibly occur when the braking maneuver has begun. We now show how the proposed strategy can handle this situation.

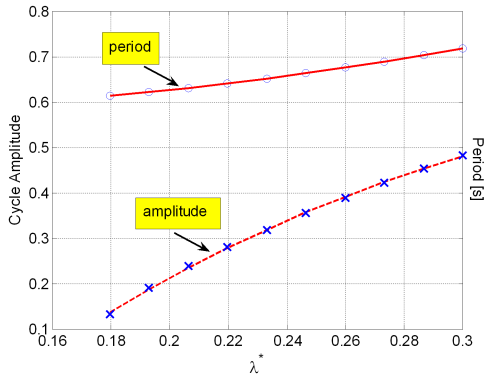

Fig. 4. Limit cycle amplitude (samples: crosses; fit: dashed line) and period (samples: circles; fit: solid line) for dry asphalt as functions of λ^*.

A. Dry-Wet μ-jump and set-point adaptation

We consider the case when a μ-jump from dry to wet asphalt occurs: based on the previous discussion, we already know how to estimate the dry road conditions and set λ^* at the bifurcation point for this type of asphalt. To manage the μ-jump from dry to wet, we analyse the relationship, for fixed road conditions, between amplitude and period of the limit cycle and the set-point value λ^*. As can be seen in Figure 4, where the limit cycle amplitude and period as functions of λ^* are shown, the data can be fitted with a parabolic curve, thus requiring three parameters only. This is true also for the relationship between λ^* and the maximum value of the braking torque θ_{Max} on the limit cycle. Thus, always with offline computations, nine matrices have been computed

$$M_{iX}(\vartheta_1, \vartheta_2) = p_i(\vartheta_1, \vartheta_2), \quad i = \{1,2,3\},\ X = \{A, T, \theta_{Max}\},$$

where $i = \{1,2,3\}$ indicates the three parameters needed to represent the parabolic fit, A, T and θ_{Max} denote the amplitude, period and maximum value of the braking torque θ_{Max} on the limit cycle, respectively, and p_i is the $i-th$ parameter of the fitting curve. The size of such matrices depends on the memory availability on the final micro-controller.

Assume now that the μ-jump from dry to wet asphalt has just occurred and that λ^* was set to the bifurcation value for dry asphalt, that is $\lambda_{Hopf,dry} = 0.166$. Once on wet road, with such a λ^* we observe a limit cycle with amplitude A_{dw}

[1] In what follows, we denote with *amplitude* the limit-cycle amplitude in λ, which can be obtained by simply monitoring the controlled variable.

and period T_{dw}. To reduce the parameter space, we need to search only for those pairs $(\vartheta_1, \vartheta_2)$ for which a limit cycle exists when $\lambda^* = 0.166$. Such a reduction can be performed by means of the already computed matrix which stores the λ^*_{Hopf} for all $(\vartheta_1, \vartheta_2)$. Thus, the new road conditions are estimated as

$$(\vartheta_1^*, \vartheta_2^*) = \text{argmin}_{(\vartheta_1,\vartheta_2)}[(\overline{\text{A}} - \text{A}(\vartheta_1, \vartheta_2))^2 + (\overline{\text{T}} - \text{T}(\vartheta_1, \vartheta_2))^2 + (\overline{\theta}_{Max} - \theta_{Max}(\vartheta_1, \vartheta_2))^2]. \quad (16)$$

Figure 5 shows the estimated values of $(\vartheta_1, \vartheta_2)$ obtained

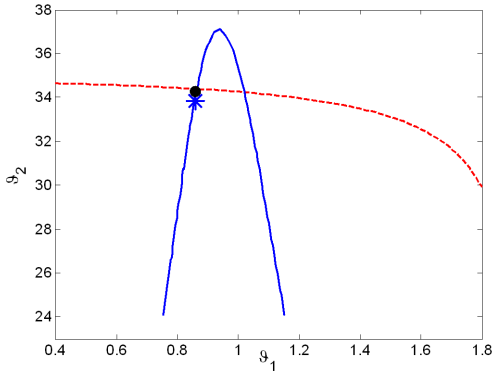

Fig. 5. True (asterisk) and estimated (dot) pair $(\vartheta_1^*, \vartheta_2^*)$ obtained via (16) by intersecting the iso-amplitude (dashed line) and iso-period (solid line) curves when a dry-to-wet μ-jump occurs.

via (16) when a dry-to-wet μ-jump occurs. For readability, only the iso-amplitude and iso-period curves are shown in Figure 5. Again, the error component of (16) which accounts for the maximum value of the braking torque θ_{Max} on the limit cycle is crucial to find the estimate of the correct point. Notably, the percentage relative estimation error obtained - with matrices of size 70×70 - is of 0.001% for ϑ_1 and ϑ_3 and 1.3% for ϑ_2. Once the asphalt has been estimated, by means again of the matrix which stores λ^*_{Hopf} for all $(\vartheta_1, \vartheta_2)$, the new optimal set-point value is set.

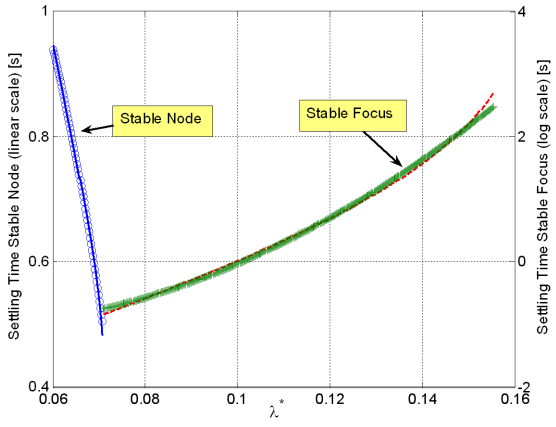

Fig. 6. Settling time for the stable node (samples: circles, fit: solid line) in linear scale and for the stable focus (samples: crosses, fit: dashed line) in logarithmic scale as functions of λ^* on dry asphalt.

B. Wet-Dry μ-jump and set-point adaptation

When moving from wet to dry asphalt, assuming that the μ-jump occurs when the system was operating at $\lambda^*_{Hopf,wet}$, on the new road conditions – according to Proposition 4.1 – a transient to an asymptotically stable equilibrium point will be observed. Let t_t be the time interval needed to reach this new stationary condition. Thus, t_t can be approximated as $t_t \simeq 5\tau_d = 5/|\max[Re(\sigma_i)]|$, where σ_i are the eigenvalues of the Jacobian matrix evaluated at the newly reached equilibrium. The nature of the transient depends on the type of the new equilibrium point: it can be either a stable node or a stable focus. In fact, as λ^* approaches λ^*_{Hopf} from the left, we first have a stable node, then the real eigenvalues coincide and a stable focus arises, which is maintained until λ^*_{Hopf} is reached and the eigenvalues become purely imaginary. According to the nature of the equilibrium (which can be evaluated on-line by simply plugging the equilibrium values into the eigenvalues expression), we can evaluate t_t as

$$t_t = t_{\mu-jump} - t_f, \quad t_f : \frac{d\theta}{dt} < \varepsilon, \quad 0 < \varepsilon < \overline{T}_b, \quad (17)$$

where $t_{\mu-jump}$ is the time instant when the change of asphalt occurs, and t_f is the fist time instant when the condition on the time derivative of the braking torque is satisfied. A suitable value for ε was found to be 0.005. Again, we analyse the relationship between t_t and the set-point value λ^*. As can be seen in Figure 6, where t_t as a function of λ^* is shown both for the stable node and the stable focus case, the data can be fitted with a parabolic curve. Specifically, to obtain a parabolic relationship for the stable focus case t_t has to be evaluated on a logarithmic scale. This is due to the fact that, for a second order system with complex conjugate poles, the envelope of the step response is given by $Y_e = 1 \pm e^{\text{Re}(\sigma_i)t}$. Thus, with off-line computations, six new matrices have been built, which store the coefficients of the fitting curves for the chosen grid of $(\vartheta_1, \vartheta_2)$. Based on these data, after the μ-jump occurred and the system settled to the new equilibrium, the pair $(\vartheta_1, \vartheta_2)$ corresponding to the estimated t_t is found. Having considered only a single parameter t_t, this analysis identifies a curve - and not a single point - in the parameter space $(\vartheta_1, \vartheta_2)$. To find the pair corresponding to the new dry road conditions, a second factor needs to be considered, that is the new equilibrium value of the control variable θ^*. As such, one needs to evaluate – in this case for $\lambda^*_{Hopf,wet}$ – the equilibrium values of θ^* for the considered pairs $(\vartheta_1, \vartheta_2)$. Doing this, thus searching for

$$(\vartheta_1^*, \vartheta_2^*) = \text{argmin}_{(\vartheta_1,\vartheta_2)}[(\bar{\text{t}}_\text{t} - \text{t}_\text{t}(\vartheta_1, \vartheta_2)^2 + (\overline{\theta}^* - \theta^*(\vartheta_1, \vartheta_2))^2],$$

one finds the point of intersection between the curves, that is $t_t(\vartheta_1, \vartheta_2; \lambda^*_{Hopf,wet})$ and $\theta^*(\vartheta_1, \vartheta_2; \lambda^*_{Hopf,wet})$. The relative percentage estimation error - with all matrices of size 70×70 - is of 0.005% for ϑ_1 and ϑ_3 and 0.3% for ϑ_2.

VII. Bifurcation Analysis and Braking Performance Degradation

Bifurcation theory offers powerful tools to analyse how the closed-loop behavior of a system may vary in face of possible perturbations in the parameters. For the application

at hand, it is of particular interest to investigate the nature of the closed-loop trajectories when the braking system undergoes faults or performance degradation which can be due to usage. The analysis can be performed via a bifurcation diagram made with respect to the set-point value λ^* and to the upper bound of the braking torque $\overline{T}_b$. In fact, the controller has been developed assuming – in particular – that $\overline{T}_b > \max_\lambda \Psi(\lambda)$. Now, the case in which $\overline{T}_b$ may vary due to undesired events is considered, and the bifurcation diagram in the parameters space $(\lambda^*, \overline{T}_b)$ (see Figure 7) is built. This diagram shows that there are seven different regions in the parameters space separated by four bifurcation curves. The bifurcations which can occur are: a Hopf bifurcation (solid line in Figure 7), saddle-node bifurcations (dashed line in Figure 7) and trans-critical bifurcations (dotted lines in Figure 7). From the asymptotic behavior viewpoint, the

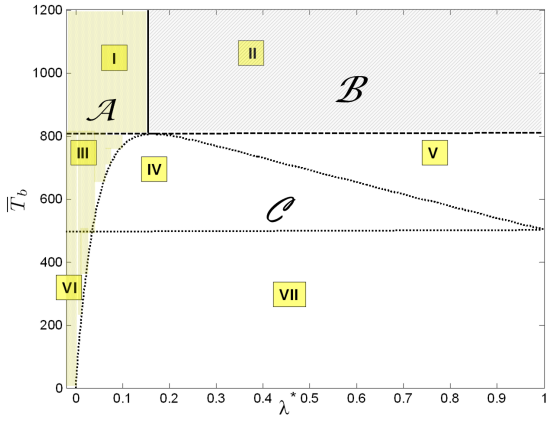

Fig. 7. Bifurcation diagram in the parameter space $(\lambda^*, \overline{T}_b)$ for dry asphalt: Hopf (solid line), saddle-node (dashed line) and transcritical bifurcation (dotted line) curves.

seven regions can be grouped as follows (see also Figure 7). $\mathscr{A} = \{I, III, VI\}$: all closed-loop system trajectories evolve towards the equilibrium $(\lambda^*, \Psi(\lambda^*))$. $\mathscr{B} = \{II\}$: the closed-loop system trajectories evolve towards an attractive periodic orbit. $\mathscr{C} = \{IV, V, VII\}$. The closed-loop system trajectories evolve towards the equilibrium $(\overline{\lambda}, \overline{T}_b)$ with $\Psi(\overline{\lambda}) = \overline{T}_b$. In this case, the choice of the set-point λ^* does not influence the closed-loop behavior, which is determined only by the intersections between the trapping region (9) and the curve $\Psi(\lambda)$.

From the braking performance view-point, if we assume that the braking system undergoes a fault or a degradation due to usage, this means that the upper bound on the admissible braking torque $\overline{T}_b$ decreases. According to the set-point value λ^*, this implies that - in the parameter space - we move either from region $\mathscr{A}$ to region $\mathscr{C}$ or from region $\mathscr{B}$ to region $\mathscr{C}$. Based on the bifurcation analysis, the only potentially dangerous situation occurs when the latter happens. In fact, when the bifurcation curve from region *II* to region *V* is crossed, there is a saddle-node bifurcation in which the two equilibria - a saddle and an unstable node - on the boundary of region V collide and disappear in region II. The collision occurs on the cycle which exists

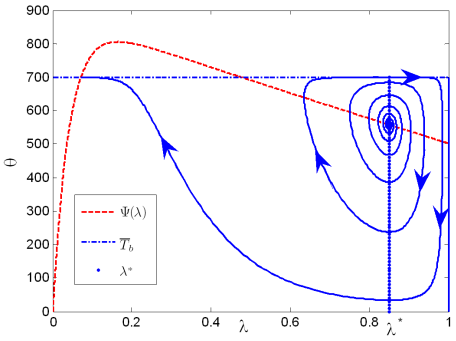

Fig. 8. Phase portrait of the closed-loop system in region V, with $\lambda^* = 0.85$ and $\overline{T}_b = 700$Nm on dry asphalt and with initial conditions $\lambda(0) = 0.85, \theta(0) = 560$Nm.

in region II and disappears via heteroclinic connection. The cycle is heteroclinic because it contains portions of the trajectories connecting the saddle point $(1,0)$ and $(1,\overline{T}_b)$. This is therefore a saddle-node bifurcation on a heteroclinic cycle. Thus, in this situation, the system might come close to the locked wheel condition. This can be appreciated by inspecting Figure 8, where a phase portrait of the closed-loop system in region V on dry asphalt is shown. The closed-loop trajectory, even though in the end converges to the *safe* equilibrium point $(\overline{\lambda}, \overline{T}_b)$, gets close to wheel locking. This analysis suggests that, if a gradual degradation of the braking performance is observed, a sensible strategy would be to switch to a fixed set-point value placed to the left of the peak of the friction curve for all road conditions. This would make the performance sub-optimal but guarantee passengers' safety.

REFERENCES

[1] D. K. B. Hassard and Y. Wan, *Theory and Applications of Hopf Bifurcations*. Cambridge University Press, Cambridge, UK, 1981.
[2] C. Canudas de Wit, M. Petersen, and A. Shiriaev, "A new nonlinear observer for tire/road distributed contact friction," in *Proceedings of the 42nd IEEE Conference on Decision and Control, Maui, Hawaii USA*, 2003.
[3] S. Drakunov, U. Ozguner, P. Dix, and B. Ashrafi, "ABS control using optimum search via sliding modes," *IEEE Transactions on Control Systems Technology*, vol. 3, no. 1, pp. 79–85, 1995.
[4] J. Guckenheimer and P. Holmes, *Nonlinear Oscillations, Dynamical Systems, and Bifurcations of Vector Fields*. Springer-Verlag, New York, 2002.
[5] F. Gustafsson, "Slip-based tire-road friction estimation," *Automatica*, vol. 33, no. 6, pp. 1087–1099, 1997.
[6] T. Johansen, I. Petersen, J. Kalkkuhl, and J. Lüdemann, "Gain-scheduled wheel slip control in automotive brake systems," *IEEE Transactions on Control Systems Technology*, vol. 11, no. 6, pp. 799–811, November 2003.
[7] U. Kiencke and L. Nielsen, *Automotive Control Systems*. Springer-Verlag, Berlin, 2000.
[8] Y. Kuznetsov, *Elements of Applied Bifurcation Theory*. Springer-Verlag, New York, 1995.
[9] E. Ono, K. Asano, M. Sugai, S. Ito, M. Yamamoto, M. Sawada, and Y. Yasui, "Estimation of automotive tire force characteristics using wheel velocity," *Control Engineering Practice*, vol. 11, pp. 1361–1370, 2003.
[10] S. Savaresi, M. Tanelli, and C. Cantoni, "Mixed Slip-Deceleration Control in Automotive Braking Systems," *ASME Journal of Dynamic Systems, Measurement and Control*, vol. 129, no. 1, pp. 20–31, 2006.
[11] M. Tanelli, A. Astolfi, and S. Savaresi, "Robust nonlinear output feedback control for brake-by-wire control systems." *Automatica*, vol. 44, no. 4, pp. 1078–1087, 2008.
[12] S. Wiggins, *Introduction to Applied Nonlinear Dynamical Systems and Chaos*. Springer-Verlag, New York, 2003.